Beams-doc-988-v2
March 22, 2004

Cancellation of the Proton Signal on the Antiproton Cable: A Status Report

Rob Kutschke

Abstract

This note summarizes two sets of measurements which are part of a proof of principle demonstration of the proposed method to cancel the proton signal on the antiproton cable. A successful demonstration is necessary if we are to be able to measure the antiprotons in the presence of protons and, later, to measure the protons in the presence of high intensity antiprotons. This note will demonstrate that we have a high quality antiproton signal but that significant calibration issues remain.

Contents

1 Introduction

In the first study presented here, dedicated study time was used to move the beam in both the horizontal and vertical directions. During this study one horizontal BPM and one vertical BPM were instrumented with hew electronics. The data recorded with the new electronics will be used to derive a function which describes the proton signal on the antiproton cables as a function of the proton signal on the proton cables. The correction algorithm developed in this study will be used in the second study.

One of the major difficulties in demonstrating correctly calibrated antiproton measurements with the new BPM electronics is that there is no well calibrated reference against which to compare the measurements. There is, however, a time during a shot setup that it is possible to make an accurate prediction of the $\bar{p}$ position. In the second study one horizontal BPM was instrumented with the new electronics which were used to record the BPM signals during a shot setup. This allows us to compare the measured and predicted $\bar{p}$ positions.

1.1 Predicting the $\bar{p}$ Position during Shot Setup

The interesting time during shot setup is the following,

1) No beam in machine. Helix closed. Inject protons onto central orbit at 150 GeV.

2) Open the helix. The protons are now on the proton helix at 150 GeV.

3) Inject the antiprotons onto the antiproton helix, at 150 GeV.

We also need to make several assumptions:

A1) The central orbit does not change when the helix opens.

A2) The central orbit does not change during antiproton injection.

A3) The protons and antiprotons see essentially the same fields throughout their orbits so that the offsets of the two helices, relative to the central orbit, are equal and opposite.

A4) For now we will assume that the position is linear in $(A-B)/(A+B)$. This model will be improved in a later study.

If these assumptions are true, then we can predict the antiproton position: [1]

$$\begin{aligned} x_{\bar{p}\,predicted} &= x_{p\,\text{central}} - (x_{p\,\text{helix}} - x_{p\,\text{central}}) \\ &= 2\,x_{p\,\text{central}} - x_{p\,\text{helix}}, \end{aligned} \tag{1}$$

[1] Throughout this note we will discuss a BPM which measures horizontal position. The same considerations, and similar equations, apply for a BPM which measures vertical position.

where $x_{p\ \mathrm{central}}$ is the proton position measured while the proton beam is on the central orbit, case 1) above, and where $x_{p\ \mathrm{helix}}$ is the proton position measured when the proton beam is on the proton helix, case 2) above. There is no clean way to monitor the above assumptions but some confidence can be had in the second assumption by checking that the proton position is stable during the antiproton injection.

2 The Experimental Setup

The measurements reported here were performed using the BPM HA15 which was removed from normal Tevatron operations and was dedicated to these studies. All 4 signals from the BPM, A_p, $A_{\bar{p}}$, B_p and $B_{\bar{p}}$, were sent to the A1 house and connected to a spare electronics board from the Main Injector damper system (damper board). The cables were phase matched at the RF frequency ($\simeq 53.1$ MHz) in pairs, (A_p, B_p) and $(A_{\bar{p}}, B_{\bar{p}})$. There was no attempt to phase match the $\bar{p}$ pair with the p pair. The configuration is shown in figure 1.

The damper boards were used for this study because they report the down-converter output for each of the 4 channels, information which is necessary to study cancellation of the proton signals on the antiproton cables. The other boards being studied, including the technology choice, the recycler Echotek board, report more highly processed information from which the required information cannot be recovered. An effort is currently underway to modify a spare recycler Echotek board to report the required quantities. Difference between this system and the system described in our technology choice [1] are summarized in table 1.

The damper boards were configured to take data about once every 8 seconds and to write this data to disk. The contents of one of these files is described in appendix A. These files were processed offline, as described in appendix B, to produce one complex number for each channel. This complex number is the Fourier component, at the RF frequency, for the 9.7 turns of data on that channel. The net result of the system is four complex numbers, $\{\mathbf{A_p}, \mathbf{B_p}, \mathbf{A_{\bar{p}}}, \mathbf{B_{\bar{p}}}\}$, every 8 seconds.

For the first measurement, the BPM VA15 was also taken out of normal Tevatron operations and dedicated to this study. Again all four signals were sent from the BPM and connected to electronics in the A1 house. In this case the electronics was a recycler Echotek board. It was configured to report the vertical position of the beam about once per second. It does not report phase information and, therefore, cannot be used to study cancellation of the proton signal on the antiproton cable. This configuration is described in more detail in Beams-doc-967.

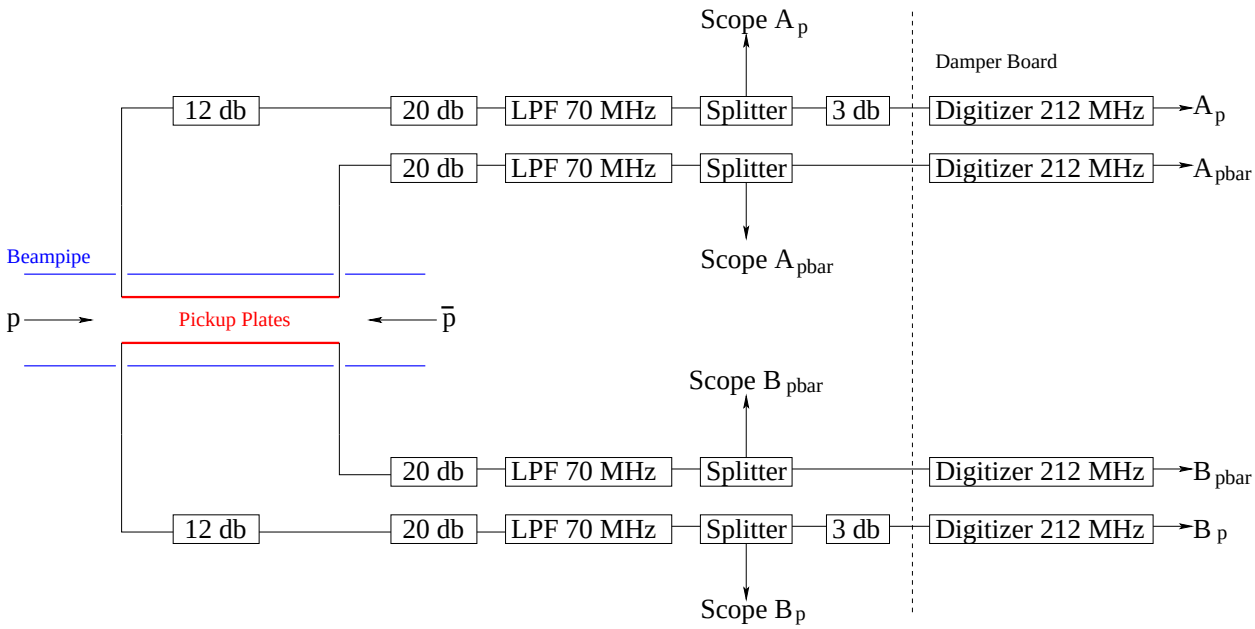

Figure 1: Configuration of the BPM and damper board used for these measurements. The attenuators were chosen to match, approximately, the signals to the full range of the damper board digitizers. The additional 12 db in the proton line partly compensates for the higher intensity of the proton beam relative to the antiproton beam. The boxes labeled LPF are low pass filters. The additional 3db attenuator in the line from the splitter to the damper board reduces a reflection which is produced by improper termination of the proton cables. Because of the lower $\bar{p}$ intensity, the corresponding reflection from the improper termination of the $\bar{p}$ cables is too small to be important. The data from the scope inputs were used in a separate study and will not be discussed here.

Property	Damper Board	Modified Recycler Echotek
Sampling Frequency	$4 \times$ RF ($\simeq$ 212 MHz)	$7/5 \times$ RF ($\simeq$ 74 MHz)
Number of ADC bits	12	14
Resolution bandwidth	$\simeq$ 5 kHz	$\simeq$ 1 kHz
Number of turns	$\simeq$ 9.7	$\simeq$ 50

Table 1: Comparison of properties of the damper board with those of the current technology choice[1], a modified recycler Echotek board. The final row reports the number of turns of data which are added coherently to form the I and Q outputs; this information is equivalent to that contained in the resolution bandwidth.

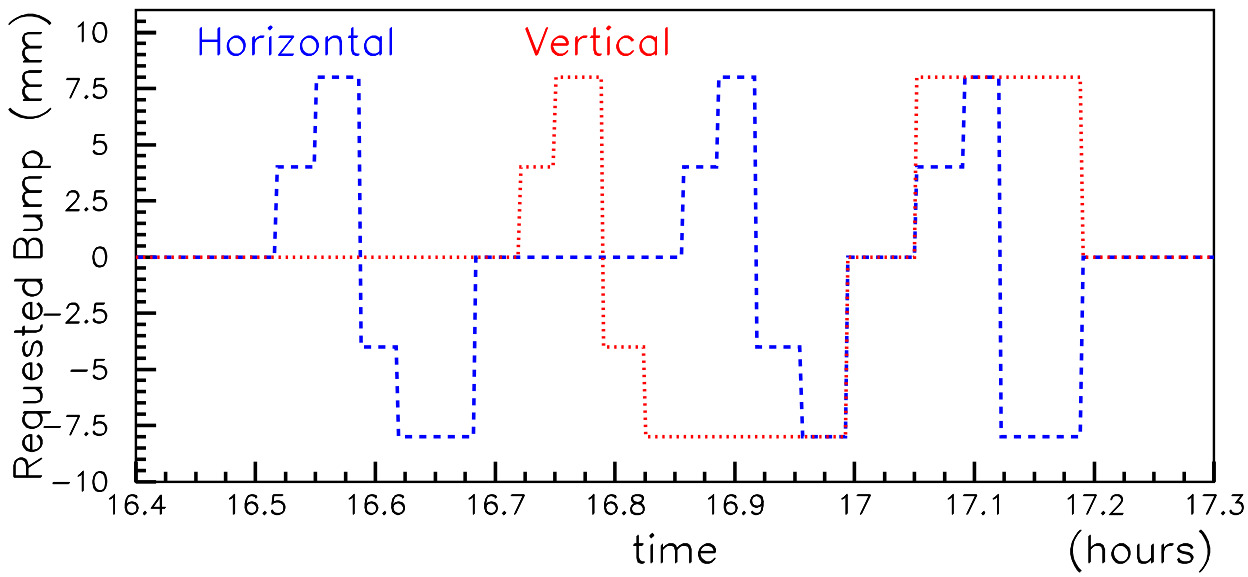

Figure 2: The requested bumps, horizontal bump at HA15 and vertical bump at VA14, for the study of January 10, 2004.

3 Building a Model of the p Signal on the $\bar{p}$ Cables

The study reported here used data taken on Jan. 10, 2004 between 3:56 PM and 5:35 PM. The bunch configuration was proton only 12×0. The horizontal position was measured with a damper board at HA15 and the vertical position was measured with a recycler Echotek at VA15.

During this study bumps were introduced at HA15 and VA15. The details of the bumps are recorded in a table in Beams-doc-987 and graphically in figure 2.

The proton horizontal position at HA15 was computed using the damper board data,

$$x_p = 26 \frac{|\mathbf{B_p}| - |\mathbf{A_p}|}{|\mathbf{B_p}| + |\mathbf{A_p}|}, \tag{2}$$

where $\mathbf{A_p}$ and $\mathbf{B_p}$ are the complex numbers described in the previous section and the appendices, and where 26 is the factor which turns the ratio into a position in mm. For now any nonlinearities in the transformation from the ratio to position will be ignored. The proton vertical position at VA15 was taken from a file sent to me by Bob Webber. The computation of these positions is described in Beams-doc-987.

These measured positions are shown in figure 3. There is an offset between the set and measured positions but this is not important because the set position is the size of a bump relative to the original orbit; it is not an absolute number.

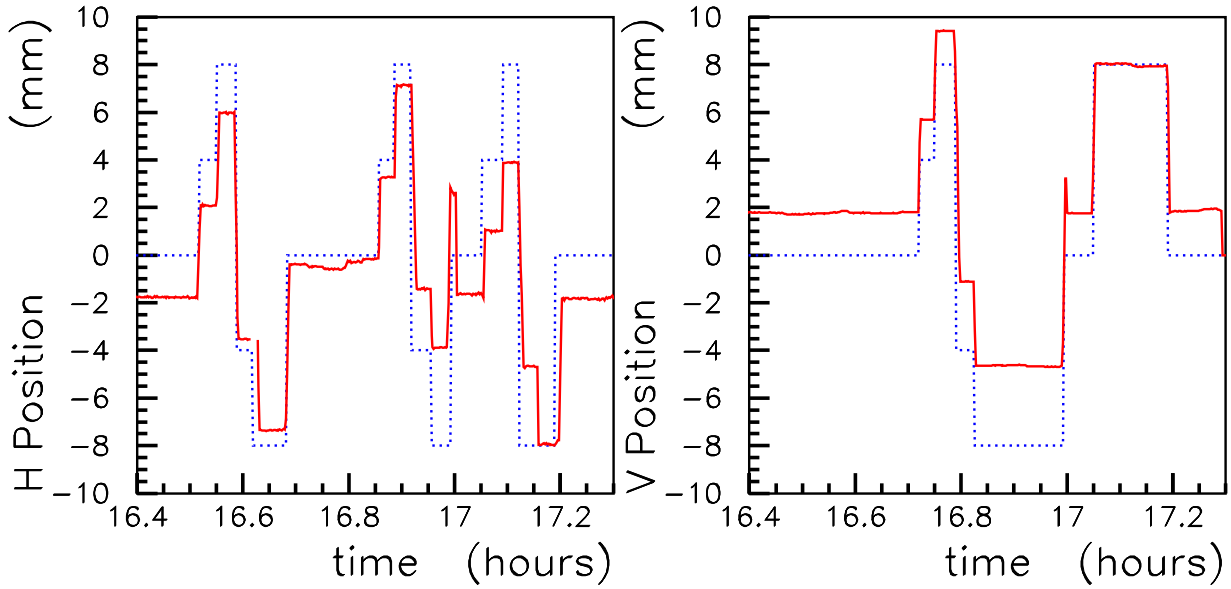

Figure 3: Measured positions at HA15 and VA14 (solid red lines) with the bump setting (dotted blue lines) overlayed. The gap in the measured horizontal position data near t=16.6 arises because cables were being adjusted at that time.

Qualitatively the measured beam position follows the set position but there appears to be some hysteresis in the system. For example there are two periods of time that the vertical bump is set at +8 mm. The measured positions at these times differ by about 1.5 mm. One might think that this difference arises because the beams are at different horizontal positions at these times. However this seems unlikely because, during the second of these times, the horizontal position is scanned from +8 to -8 mm and the measured vertical position varies by an amount much smaller than 1.5 mm. Bob Webber, who was in the control room for these measurements, believes that the most likely explanation is pilot error on the part of the operators. The problem is understood and can be avoided in subsequent work. This problem does not adversely affect the rest of the study presented in this note.

3.1 The First Model

Jim Steimel prepared a document, Beams-doc-884, which describes a method for canceling the proton signal on the antiproton cables. At this writing, the version of Beams-doc-884 is v1, which discusses only the approximation that there is no coupling between the plates. His equation 6, with some minor changes to notation, is,

$$A_{\bar{p}} \quad = \quad T_{\bar{p}\,p}\, I_p + T_{\bar{p}\,\bar{p}}\, I_{\bar{p}} \tag{3}$$

$$A_p = T_{p\,p}\, I_p + T_{p\,\bar{p}}\, I_{\bar{p}}, \tag{4}$$

where A_x is the observed complex signal on the x cable from the A plate, I_x beam current of species x, and where T_{xy} is the transfer function which produces an observed voltage on cable x due to current I_y. The transfer functions include the non-directionality of the pickups, attenuation in the cables and so on. A similar equation holds for the B plate. In this model, the transfer functions, T_{xy} are complex constants.

Now consider the limit that, in equation 4, $T_{p\,\bar{p}}\, I_{\bar{p}} \ll T_{p\,p}\, I_p$. In this limit,

$$\begin{aligned} A_{\bar{p}\,\mathrm{true}} &= T_{\bar{p}\,\bar{p}}\, I_{\bar{p}} \\ &= A_{\bar{p}} - T_{\bar{p}\,p}\, I_p \\ &= A_{\bar{p}} - \frac{T_{\bar{p}\,p}}{T_{p\,p}}\, A_p. \end{aligned} \tag{5}$$

The left hand side of this equation is the isolated antiproton signal which is desired. The ratio $T_{\bar{p}\,p}/T_{p\,p}$ can be measured during a proton only store. In this limit, the recipe for cancellation of the proton contamination on the antiproton cable is,

$$A_{\bar{p}\,\mathrm{true}} = A_{\bar{p}} - C_A\, A_p. \tag{6}$$

where

$$C_A = \left.\frac{A_{\bar{p}}}{A_p}\right|_{p\ only}. \tag{7}$$

The quantity C_A is complex constant, independent of time, beam position and beam intensity. It does, however, depend on the details of the materials and construction of each BPM plate and, therefore, must be determined separately for each plate. We can similarly define C_B for the B plate.

The data from January 10, 2004 have been used to test if this model is a good description of the data. The naive expectation is that deviations from the model will be seen but the size deviations is not known a priori.

Figures 4 and 5 show the behavior of the ratios $\mathbf{A_{\bar{p}}/A_p}$ and $\mathbf{B_{\bar{p}}/B_p}$ for the A and B plates of HA15. These data were taken during a proton only store so the observed ratios are a direct measure of the constants C_A and C_B in the above formalism. Figure 4 shows the magnitude of the ratios, while figure 5 shows the phases of the ratios. If these ratios were flat then the above model would be adequate to correct the $\bar{p}$ signals for the contamination from the protons. The ratios are certainly not flat; each channel has a variation of about $\pm 50\%$ of its average value.

To set the scale of significance of this variation we need to know the relative sizes of the two terms on the RHS of equation 3, $T_{\bar{p}\,p}\, I_p$ and $T_{\bar{p}\,\bar{p}}\, I_{\bar{p}}$. Appendix C shows some damper board data taken with both p and $\bar{p}$ in the machine in conditions which are typical of current operating conditions. From this we learn that these two terms are of about equal size. Therefore we need to cancel the

proton contamination which much more precision than can be achieved with this model.

The obvious next step is to try a model in which the correction depends on the proton position.

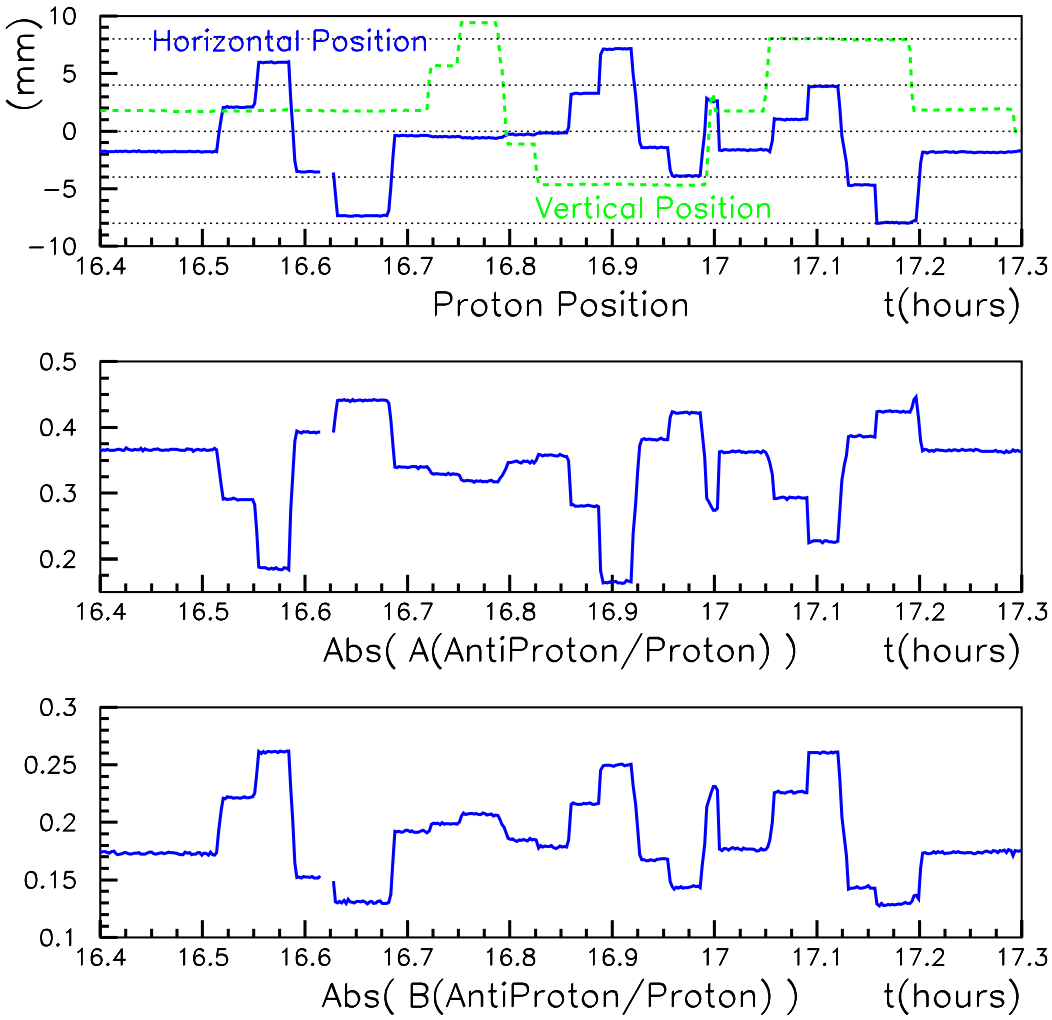

Figure 4: The top plot is provided for reference and shows the measured H and V positions that have been shown before. The middle plot shows, for the HA15 A plate, magnitude of the complex ratio $\mathbf{A}_{\bar{\mathbf{p}}}/\mathbf{A}_{\mathbf{p}}$ for a proton only store. The bottom plot shows the magnitude of the corresponding ratio for the B plate. Both ratios vary greatly as the beam positions are varied.

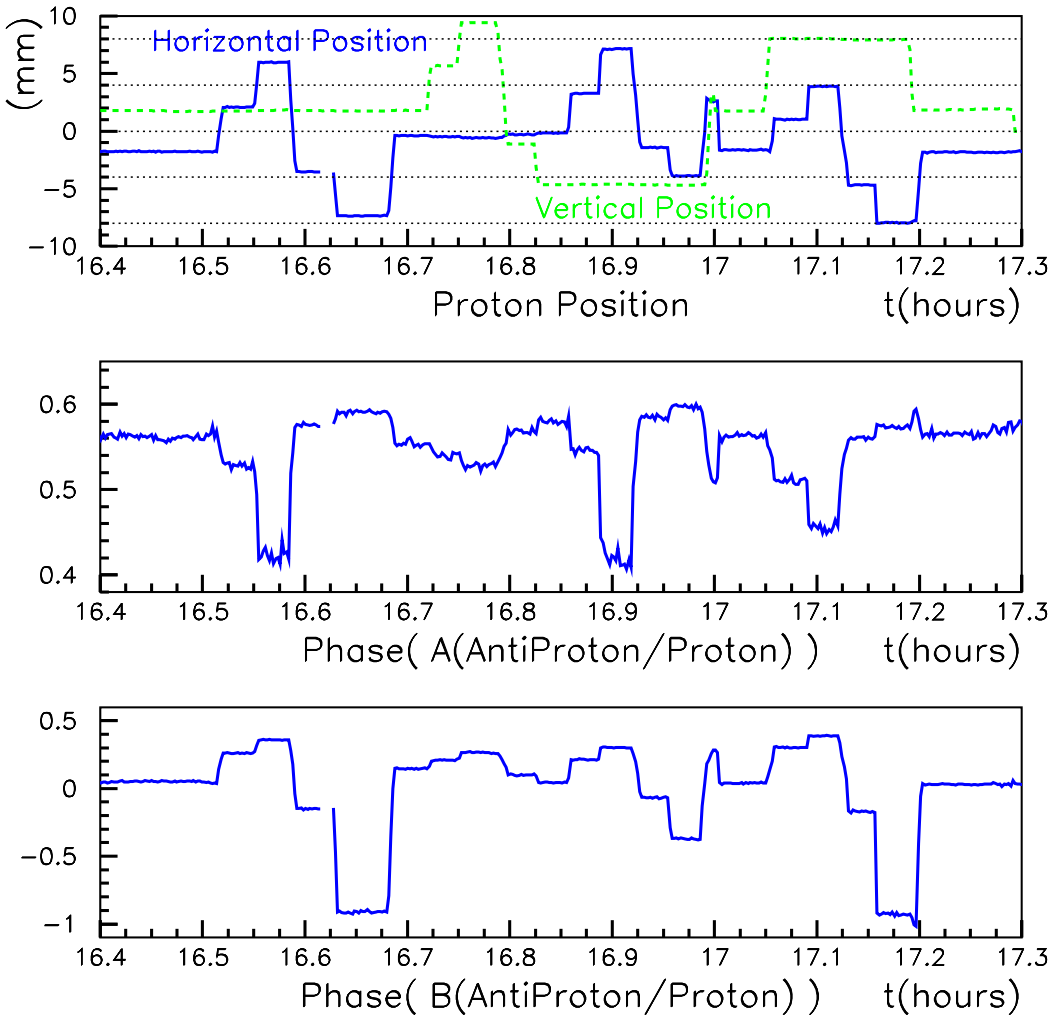

Figure 5: The top plot is provided for reference and shows the measured H and V positions that have been shown before. The middle plot shows, for the HA15 A plate, phase of the complex ratio $\mathbf{A}_{\bar{\mathbf{p}}}/\mathbf{A}_{\mathbf{p}}$ for a proton only store. The bottom plot shows the phase of the corresponding ratio for the B plate. Both phases vary greatly as the beam positions are varied.

3.2 The Second Model

The previous section showed that, contrary to the assumptions in that model, the the proton signal on the $\bar{p}$ cable does indeed depend on the proton position. In this section we will try a model in which the correction depends linearly on the **A** and **B** signals. Specifically, the corrections are,

$$\begin{aligned} \mathbf{A}_{\mathrm{cor}} &= \mathbf{a_1 A_p} + \mathbf{b_1 B_p} \\ \mathbf{B}_{\mathrm{cor}} &= \mathbf{a_2 A_p} + \mathbf{b_2 B_p} \end{aligned} \tag{8}$$

where $\mathbf{a_i}$ and $\mathbf{b_i}$ are complex constants to be determined from the data.

Figure 6 illustrates this model. The top part of the figure is again the measured horizontal and vertical position which have been previously shown. Two points at the extrema of the horizontal positions were used to determine $\mathbf{a_i}$ and $\mathbf{b_i}e$. The middle and bottom figures show, for plates A and B, the magnitude of the ratio of the corrected $\bar{p}$ signal to the uncorrected $\bar{p}$ signal,

$$\left| \frac{\mathbf{A_{\bar{p}}} - \mathbf{A}_{\mathrm{cor}}}{\mathbf{A_{\bar{p}}}} \right| \quad \text{and} \quad \left| \frac{\mathbf{B_{\bar{p}}} - \mathbf{B}_{\mathrm{cor}}}{\mathbf{B_{\bar{p}}}} \right| \tag{9}$$

In a previous version of this plot I used the proton signal, rather than the uncorrected $\bar{p}$ signal in the denominator. This changes the overall scale of the ratios but there are no other significant changes. In both the plots for both the A and B plates we see that the correction works well so long as the vertical position does not change.

From this we conclude that the correction needs to be a function of both horizontal and vertical position.

For completeness we include figure 7, which shows the phases of the complex ratios whose magnitudes were shown in figure 6. These phases show regions of instability in between 16.55 and 16.7 hours. During this time both the real and imaginary parts are, by construction, independently close to zero zero. Therefore the magnitude is well determined to be small but the phase is poorly determined. So this instability is real, understood and irrelevant.

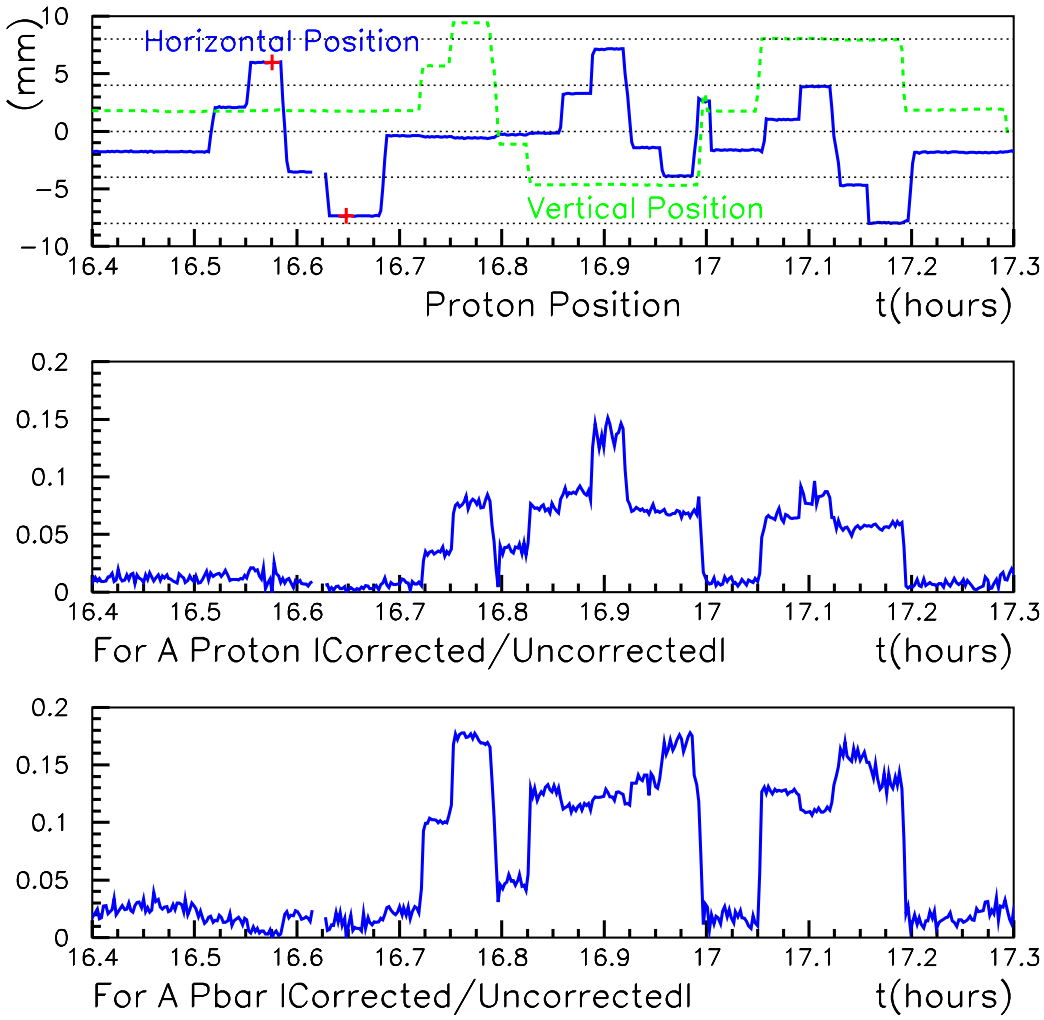

Figure 6: The top plot is provided for reference and shows the measured H and V positions that have been shown before. The two red crosses are calibration points described int the text. The middle plot shows, for the A plate, the magnitude of the ratio of corrected signal on the $\bar{p}$ cable to the uncorrected signal on the $\bar{p}$ cable, for the correction described by the third model. The bottom plot shows the same for the B plate. In previous versions of this plot the denominator was the proton signal on the proton cable.

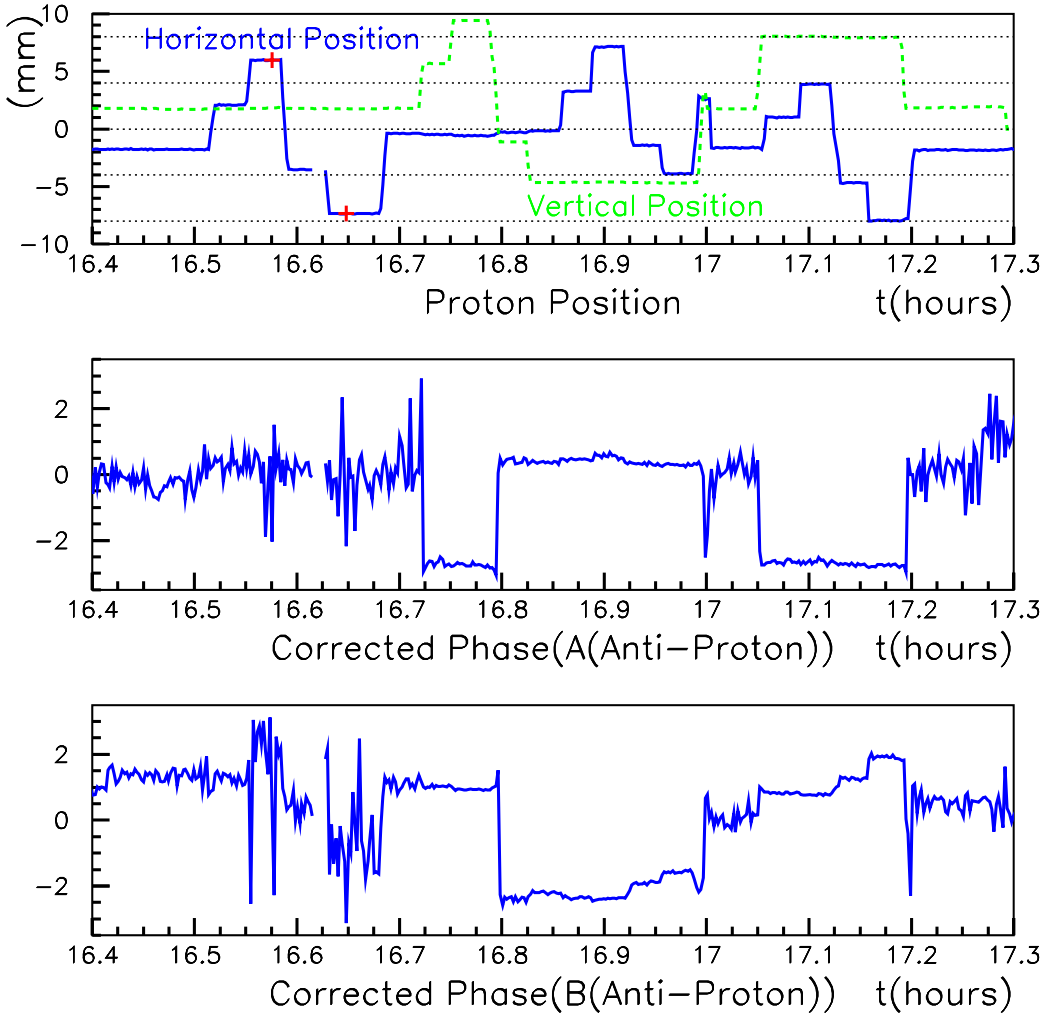

Figure 7: This figure is a companion to the previous one. It shows the phase of the ratios for which the magnitude is shown in the previous figure.

3.3 The Third Model

The previous section concluded that the correction for the proton contamination on the $\bar{p}$ cable depends on both horizontal and vertical position. The BPM under study with the damper board is HA15. While we do not have measurements of the vertical beam position at HA15, we do have measurements of the vertical beam position at a neighboring BPM, VA14. So we will parameterize the correction as a function of, y, the vertical position at VA14. The correction is,

$$\begin{aligned} \mathbf{A}_{\rm cor} &= \mathbf{a_1}(y)\mathbf{A_p} + \mathbf{b_1}(y)\mathbf{B_p} \\ \mathbf{B}_{\rm cor} &= \mathbf{a_2}(y)\mathbf{A_p} + \mathbf{b_2}(y)\mathbf{B_p}. \end{aligned} \tag{10}$$

where the complex coefficients $\mathbf{a_i}$ and $\mathbf{b_i}$ now are functions of the real parameter y. Because of the limited amount of data we will try a correction in which the coefficients depend linearly on y.

Figure 8 illustrates this correction. The top plot is the standard repeat of the measured horizontal and vertical positions during this study. The two red crosses show the points chosen to determine the parameters $\mathbf{a_i}$ and $\mathbf{b_i}$ for $y = 2$ mm and the two red X's show the points chosen to determine the parameters $\mathbf{a_i}$ and $\mathbf{b_i}$ for $y = -6$ mm.

The values of $\mathbf{a_i}$ and $\mathbf{b_i}$ for other values of y are determined by linearly interpolating or extrapolating from these values.

$$\mathbf{a_1}(y) = \mathbf{m_{a_1}} y + \mathbf{b_{a_1}}, \tag{11}$$

where $\mathbf{m_{a_1}}$ and $\mathbf{b_{a_1}}$ are complex constants determined from the two $(y, \mathbf{a_1})$ pairs computed above. Similarly for $\mathbf{a_2}$, $\mathbf{b_1}$ and $\mathbf{b_2}$.

The middle and bottom plots show, for plates A and B, the magnitude of the ratio of the corrected $\bar{p}$ signal to the uncorrected $\bar{p}$ signal,

$$\left| \frac{\mathbf{A_{\bar{p}}} - \mathbf{A}_{\rm cor}}{\mathbf{A_{\bar{p}}}} \right| \quad \text{and} \quad \left| \frac{\mathbf{B_{\bar{p}}} - \mathbf{B}_{\rm cor}}{\mathbf{B_{\bar{p}}}} \right|, \tag{12}$$

using the third model to make the correction. Compare the plots in this figure with those in figure 6, for which the correction was done with the second model. The third model makes a much more complete cancellation of the signal; the size of the residual has been reduced to about 1/3 of its previous value. Moreover, the correction works reasonably well even for values of y for which the correction requires an extrapolation.

Figure 9 shows the phase of the ratios whose magnitudes were shown in figure 8. The phases show many regions of instability. This instability is not a problem and was explained in the discussion of figure 7.

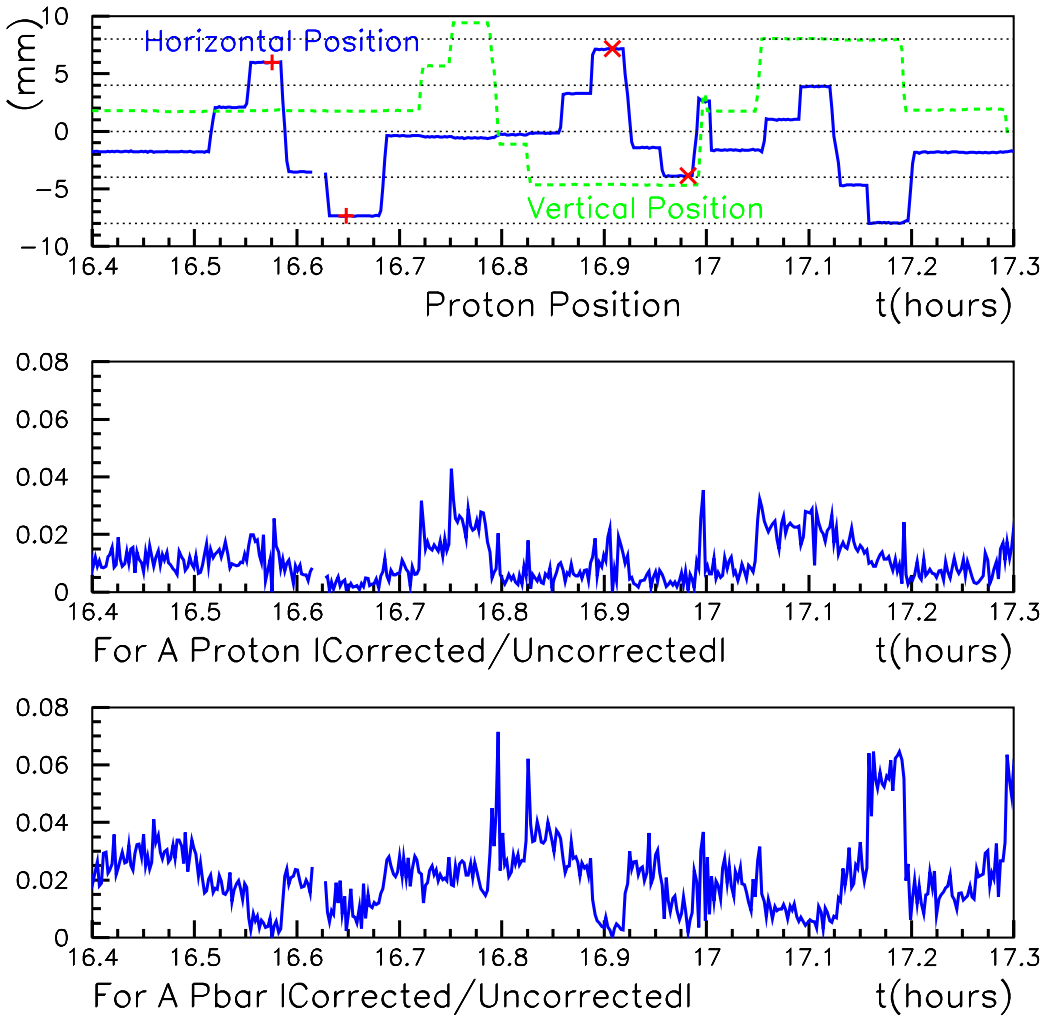

Figure 8: The top plot is provided for reference and shows the measured H and V positions that have been shown before. The two red crosses and red two X's are calibration points described int the text. The middle plot shows, for the A plate, the magnitude of the ratio of corrected $\bar{p}$ signal to the uncorrected $\bar{p}$ signal, for the third model described in the text. The bottom plot shows the same for the B plate. In previous versions of this plot the denominator was the proton signal on the proton cable.

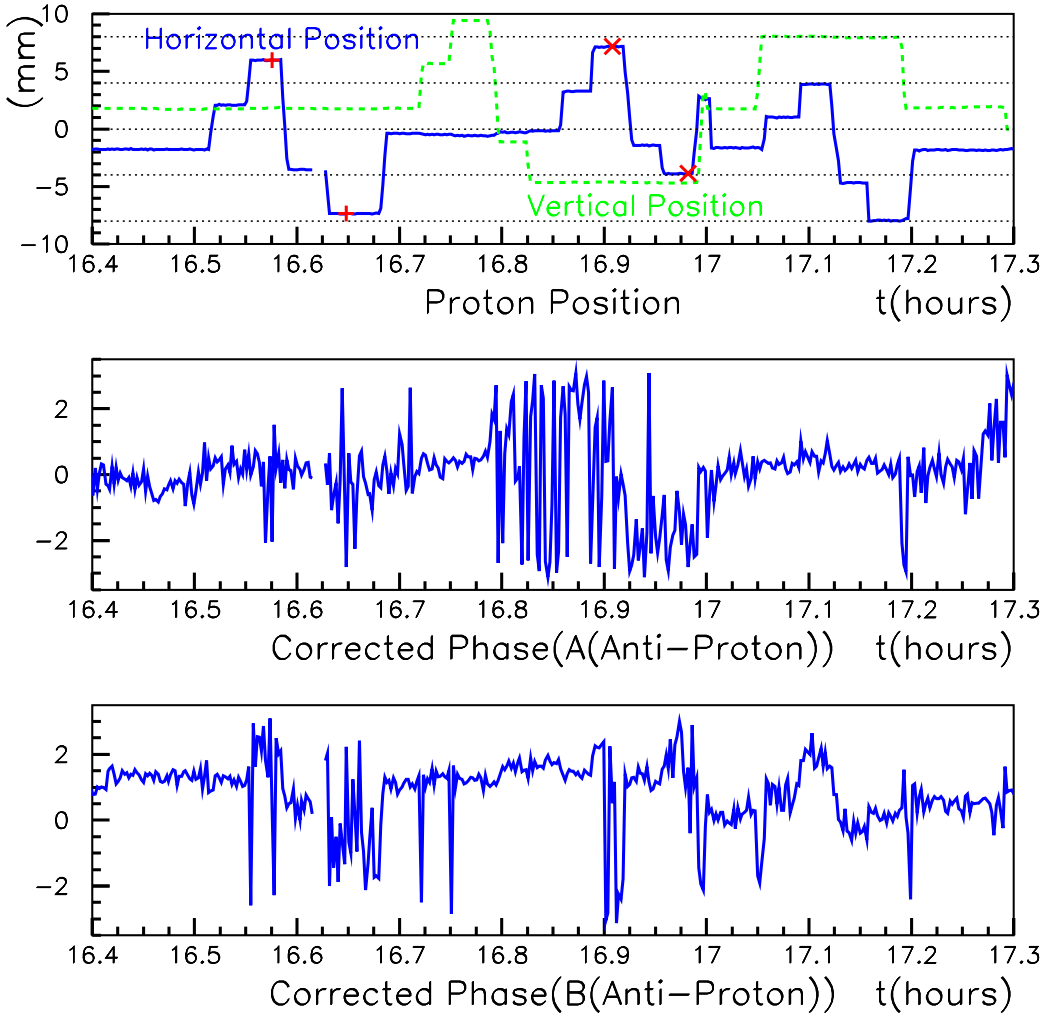

Figure 9: This plot is a companion to the previous one. It shows the phase of the ratios for which the magnitude is shown in the previous slide.

4 Looking at the Shot Set Up

On the first two pages of this note we discussed a time during shot setup when there is a good prediction of the antiproton position. In this section we will apply the correction procedure described above and see if the measured $\bar{p}$ position agrees with the prediction. Because we have no measurements of vertical position, we will use the second model, not the third, to perform the cancellation of the proton signals on the $\bar{p}$ cables.

The data used in this study were taken using the damper board on BPM HA15 during a normal shot setup on Dec. 4, 2003 between about 4:30 PM and 5:30 PM. The raw damper board data for a typical measurement is shown in appendix C.

The upper two plots in figure 10 show the magnitudes of the signals on each cable as a function of time over the course of a shot setup. The signals on the $\bar{p}$ cables are uncorrected. The left edge of the plot is in the middle of proton injection and the helix is opened just after 16.8 hours. The vertical magenta line shows the time at which $\bar{p}$ injection begins. As expected there is a significant signal on the $\bar{p}$ cable even when there are no $\bar{p}$'s in the machine. Just after 17.2 hours the $\bar{p}$ injection is completed, after which the beam is ramped, squeezed and brought into collision. The magnitude of all signals increases during the ramp because the bunches become narrower in time as the energy increases. This changes the frequency spectrum of each bunch, putting more energy into the frequency band being measured.

The middle left plot shows the sum of $|\mathbf{B_p}| + |\mathbf{A_p}|$. This is a measure of the intensity of the proton beam. The jump near 17.2 hours is an artifact due to the change of the beam energy during the ramp. We will need to develop a calibration function which takes out this dependence on the beam energy.

The middle right plot shows the proton position, as measured as

$$\text{Position} \quad = \quad 26\,(|\mathbf{B_p}| + |\mathbf{A_p}|)/(|\mathbf{B_p}| + |\mathbf{A_p}|). \tag{13}$$

Before about 16.8 hours the helix is closed and the protons are on the central orbit. Just after 16.8 hours the helix is opened and the protons move onto the proton helix. Using these two measurements we can predict the position of the $\bar{p}$ helix; relative to the central orbit it will be displaced equal and opposite to the proton helix. This prediction is drawn as the horizontal red line. The prediction is valid starting at the time of antiproton injection, which is marked by the vertical magenta line. The prediction remains valid at least until the start of the ramp. There is no reason to believe that the central orbit remains unchanged during the ramp and, without knowing the central orbit, one cannot predict the $\bar{p}$ orbit, knowing only the p orbit. This plot shows that the proton position changes during the ramp, squeeze and the start of collisions.

To correct the $\bar{p}$ signals I chose one time just before the helix opened and one time just after the helix opened. I used the data from these two times to solve for $\mathbf{a_i}$ and $\mathbf{b_i}$ in equation 8. Because I did not have information about the vertical position available, I ignored any possible change in vertical position which occured when the helix opened, during the ramp or during the squeeze.

The bottom two plots on the page are show the intensity and position signals from the corrected $\bar{p}$ signals. They will be discussed in more detail in the next section.

4.1 A First Look at Antiprotons in the Presence of Protons

The bottom row of plots in figure 10 is the ultimate goal of the work described in this note. It shows the $\bar{p}$ position and intensity signals after the subtraction of the proton contamination.

The bottom left plot shows the corrected $|\mathbf{B}_{\bar{\mathbf{p}}}| + |\mathbf{A}_{\bar{\mathbf{p}}}|$ signal. The start of $\bar{p}$ injection is indicated by the vertical magenta line and the $\bar{p}$ intensity is consistent with zero before this time. The plot shows that the $\bar{p}$ injection is done in 9 steps, with the earlier steps injecting more current than the later ones. The apparent jump in intensity near 17.2 hours is an artifact due to the change of the bunch length during the ramp. This was discussed in more detail in the previous section.

In the bottom right plot the blue curve shows the measured $\bar{p}$ position, computed as

$$\text{Position} \quad = \quad 26\,(|\mathbf{B}_{\bar{\mathbf{p}}}| + |\mathbf{A}_{\bar{\mathbf{p}}}|)/(|\mathbf{B}_{\bar{\mathbf{p}}}| + |\mathbf{A}_{\bar{\mathbf{p}}}|). \tag{14}$$

The blue curve is not drawn before the start of $\bar{p}$ injection because it is too noisy. The most striking feature is that the measured position is about 1.5 mm less than the predicted position. At present this is not understood and many possibilities need to be investigated. The next most striking feature is that the motion of the $\bar{p}$'s approximately mirrors the motion of the protons. This is good circumstantial evidence that the signal we are seeing is truly the $\bar{p}$ position.

5 Summary and Conclusions

We have shown that

1. In a typical 36×36 store, the signals on the $\bar{p}$ cables which come from the proton beam and the signals which come from the $\bar{p}$ beam are of about equal size. See appendix C.

2. We have demonstrated a technique which can cancel the proton signal on the $\bar{p}$ cable to about 1% or 2% of it self. See sections 3.2 and 3.3.

3. We have studied the relative motion of the p and $\bar{p}$ helices during a shot setup. We see a strong signal for the $\bar{p}$ position. We also set that qualitatively, and relative to the central orbit, the $\bar{p}$ helix moves equal and opposite to the p helix. See section 4.1.

4. Significant calibration issues remain.

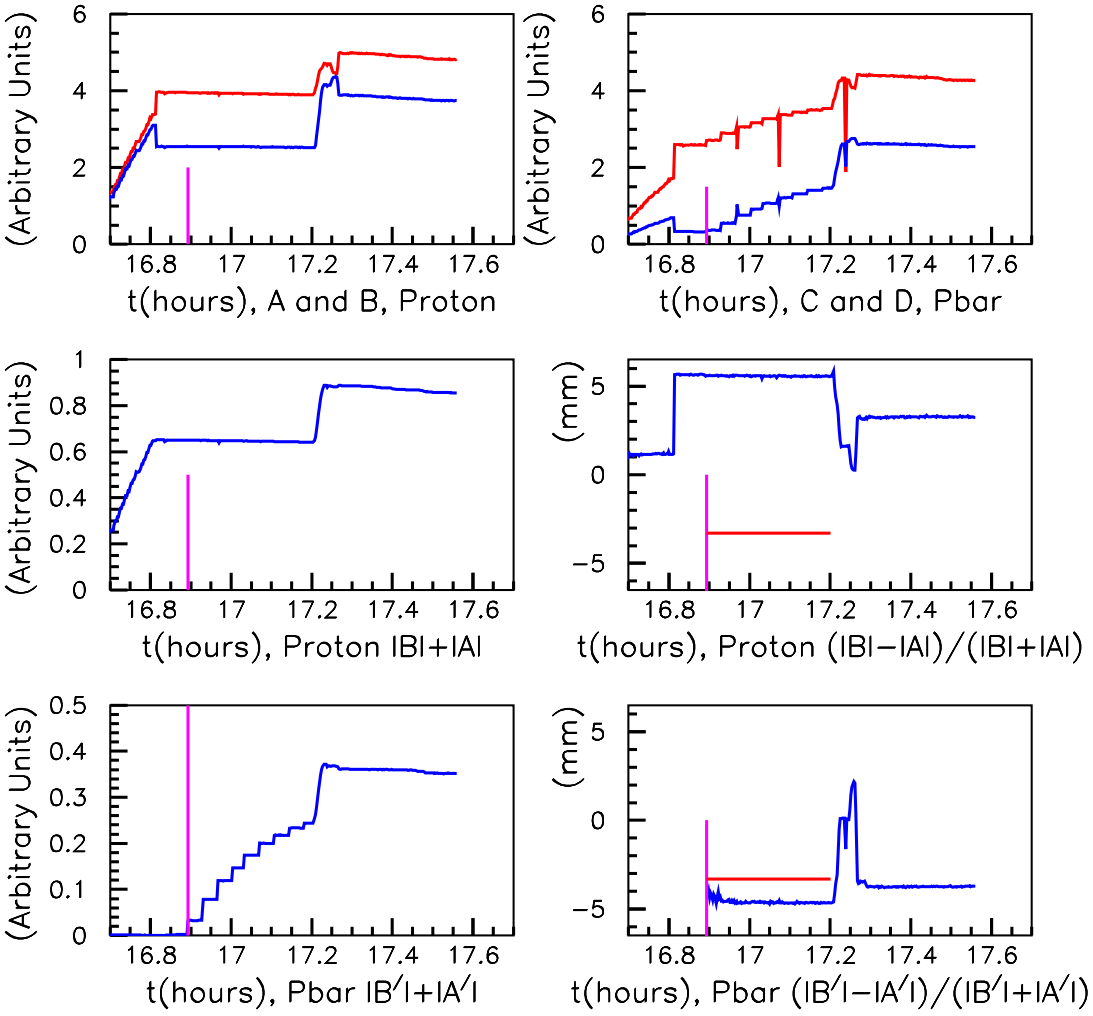

Figure 10: The top left plot shows the magnitudes of A_p and B_p during a shot setup. There is a data point approximately every 8 seconds. For all plots on this page the horizontal axis is time, in hours, from midnight on Dec. 4, 2003. The vertical magenta line shows the time at which $\bar{p}$ injection begins. The top right plot shows the magnitudes of the uncorrected $A_{\bar{p}}$ and $B_{\bar{p}}$ signals. The middle row of plots shows the $A+B$ signal and the position signal for the proton cables. The bottom row of plots shows the $A+B$ signal and the position signal for the $\bar{p}$ cables, after the correction for proton contamination. The horizontal red line on the middle right and bottom right plots shows the predicted $\bar{p}$ position, as discussed in the text.

A Contents of a Damper Board File

As configured for this study, the damper boards reports the following information:

1. Raw data: 4096 points each, A_p, $A_{\bar{p}}$, B_p and $B_{\bar{p}}$. These data have ± 11 bits and were sampled at 4 times the RF frequency. The 4096 points correspond to about 92% of one turn.

2. Digital Downconverter (DDC) output: 2048 (I, Q) pairs for each of A_p, $A_{\bar{p}}$, B_p and $B_{\bar{p}}$. This corresponds to about 9.7 turns. The algorithm used by the damper board to process the raw data into downconverted data is described below.

The damper board only stores a subset of the raw data which was used to produced the down converted data.

Several views of the raw data are shown in figures 11 and 12. There is an oddity in the data storage format: while the data has a precision as ± 11 bits, it is stored as ± 12 bits, by left shifting and setting the LSB to 0. So we see numbers in the range of [-4096,4095], even though we expect to see [-2048,2047]. It appears that the prompt signal on the $\bar{p}$ cable comes about 35 ns before the signal on the p cable. However the p and $\bar{p}$ cables are not phase matched so this timing difference is meaningless. The reflected signal on the $\bar{p}$ cable comes about 85 ticks, or 400 ns after the associated prompt pulse. This implies that the p cable run from the BPM to the house is about 200 ns, or about 80 m, assuming a propagation speed in the cable of about $0.75c$. This seems reasonable.

Inspection of the raw data shows that the ratio of the peak signal on the p cable to the peak of the prompt signal on the $\bar{p}$ cable is about 5.65 (3000/750), where the factor of 5.65 comes from the additional 15 db of attenuation in the p cable relative to the $\bar{p}$ cable, This implies a directionality of about 4.4%.

Should include a reference to see if this this makes sense? Should also redo this using the downconverted data, not the raw data.

The digital downconverter (DDC) on the damper board produces new output every 21 ticks of the sampling clock, approximately once every 99 ns. The nth output is given by,

$$I_n(R) = \sum_{i=21n-62}^{21n} R_i \cos \omega_r t_i \tag{15}$$

$$Q_n(R) = -\sum_{i=21n-62}^{21n} R_i \sin \omega_r t_i \tag{16}$$

where R is one of the raw data arrays, $\{A_p, A_{\bar{p}}, B_p, B_{\bar{p}}\}$, i is an index into one of these arrays, $\omega_r = 2\pi f_r$ and where f_r is a reference frequency. Therefore I and Q are just the Fourier cosine and sine transforms, evaluated at f_r. In the damper board f_r is the RF frequency which is, by construction, exactly 1/4 of

the sampling frequency. Therefore all of the sines and cosines are just 0 or ± 1. The notation I and Q stands for "In phase" and "Quadrature".

Careful reading of the summation range shows that the algorithm uses 63 raw data points, then shifts 21 points and repeats. Therefore, each point in the downconverter output shares 2/3 of its data with each of its nearest neighbors and 1/3 of its data with each of its next nearest neighbors.

I am not 100% certain of the conventions in use in this field. For example I could have swapped the definitions of I and Q, or blown a sign in one of their definitions. This makes no difference to the final result so long as a consistent convention is used throughout.

Figures 13 and 14 show the outputs of the DDC for about 1.3 turns of these data.

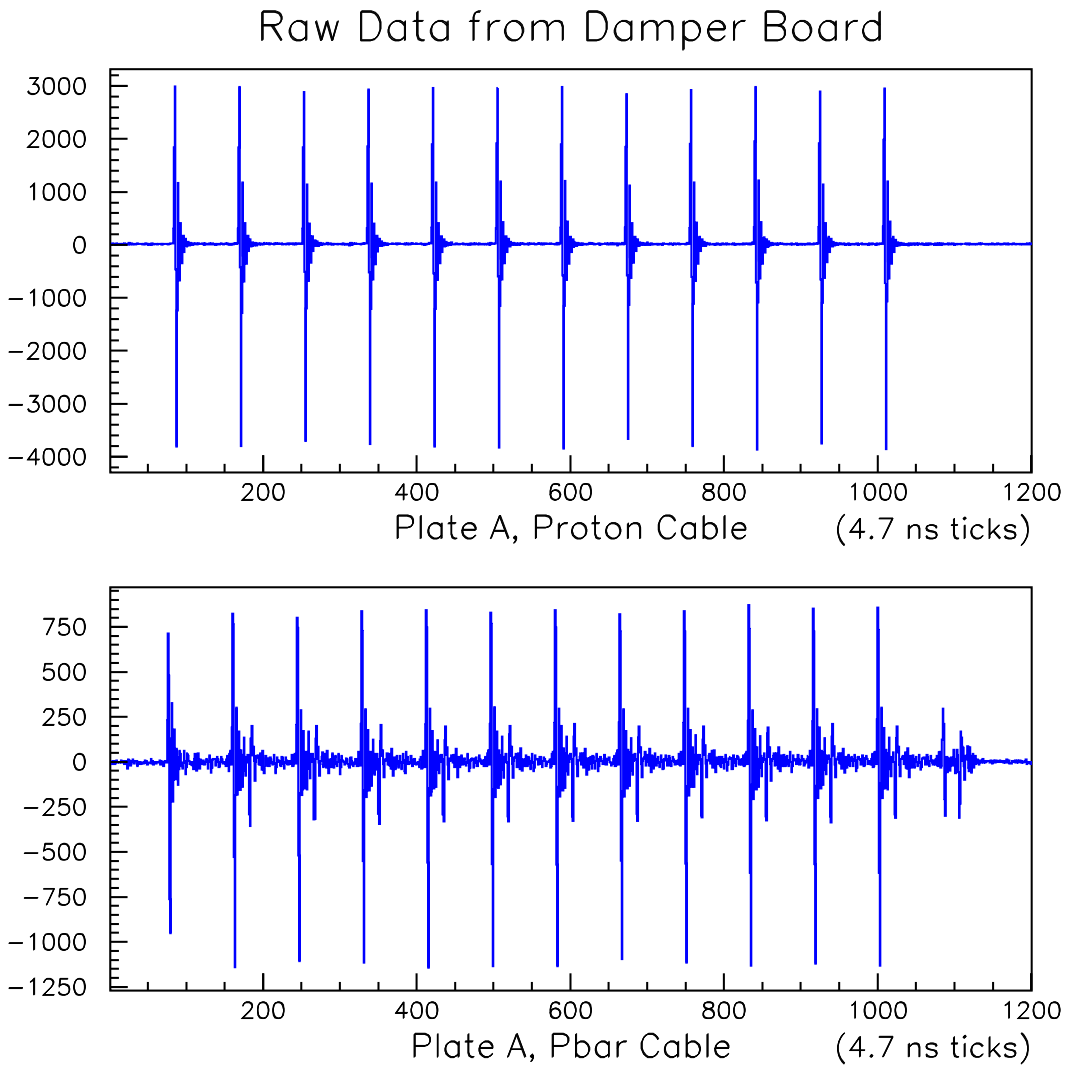

Figure 11: Raw data from the damper board, showing data for one train of 12 bunches of protons from a 12×0 proton only store. The horizontal axis is time, in units of ticks of the digitization clock and the vertical axis is $2\times$ the counts on a ± 11 bit ADC (see text for details). The full time scale is 27% of one turn. The signals on the $\bar{p}$ cable include the prompt non-directional component plus a reflection from an improper termination of the proton cable. This will be further discussed in figure 12.

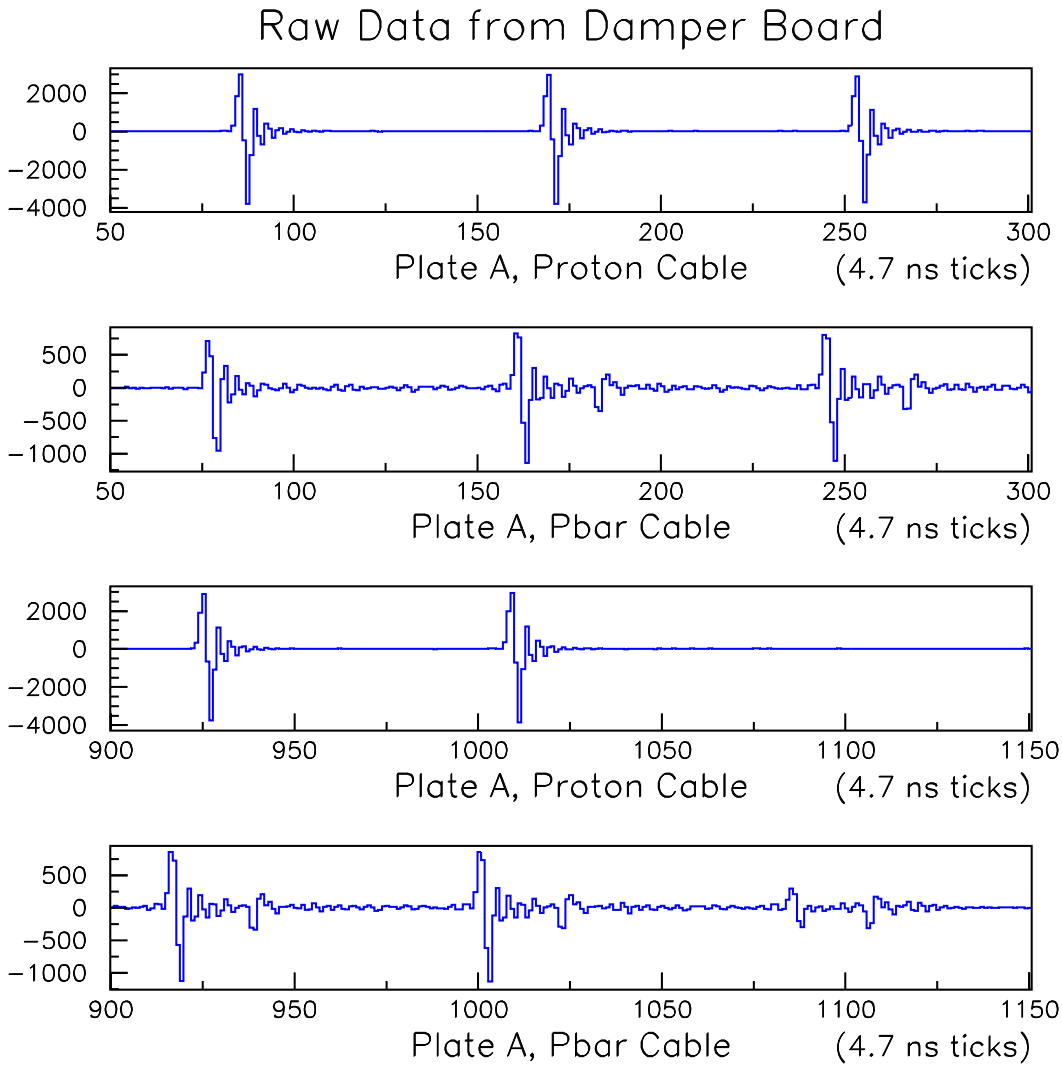

Figure 12: A zoomed in view of the raw data from figure 11. These figures show the first three bunches and the last two bunches from each of the trains. The p and $\bar{p}$ cables are not phase matched. The first signal on the $\bar{p}$ cable, near 75 ticks, is the prompt, non-directional signal from the first proton bunch. The last structure on the $\bar{p}$ cable, the doublet from about 1080 to 1120 ticks, is the reflected signal due to improper termination of the proton cable. The other structures on the $\bar{p}$ cable are the sum of the two; by accident the round trip delay of the reflected signal is about equal to the bunch spacing.

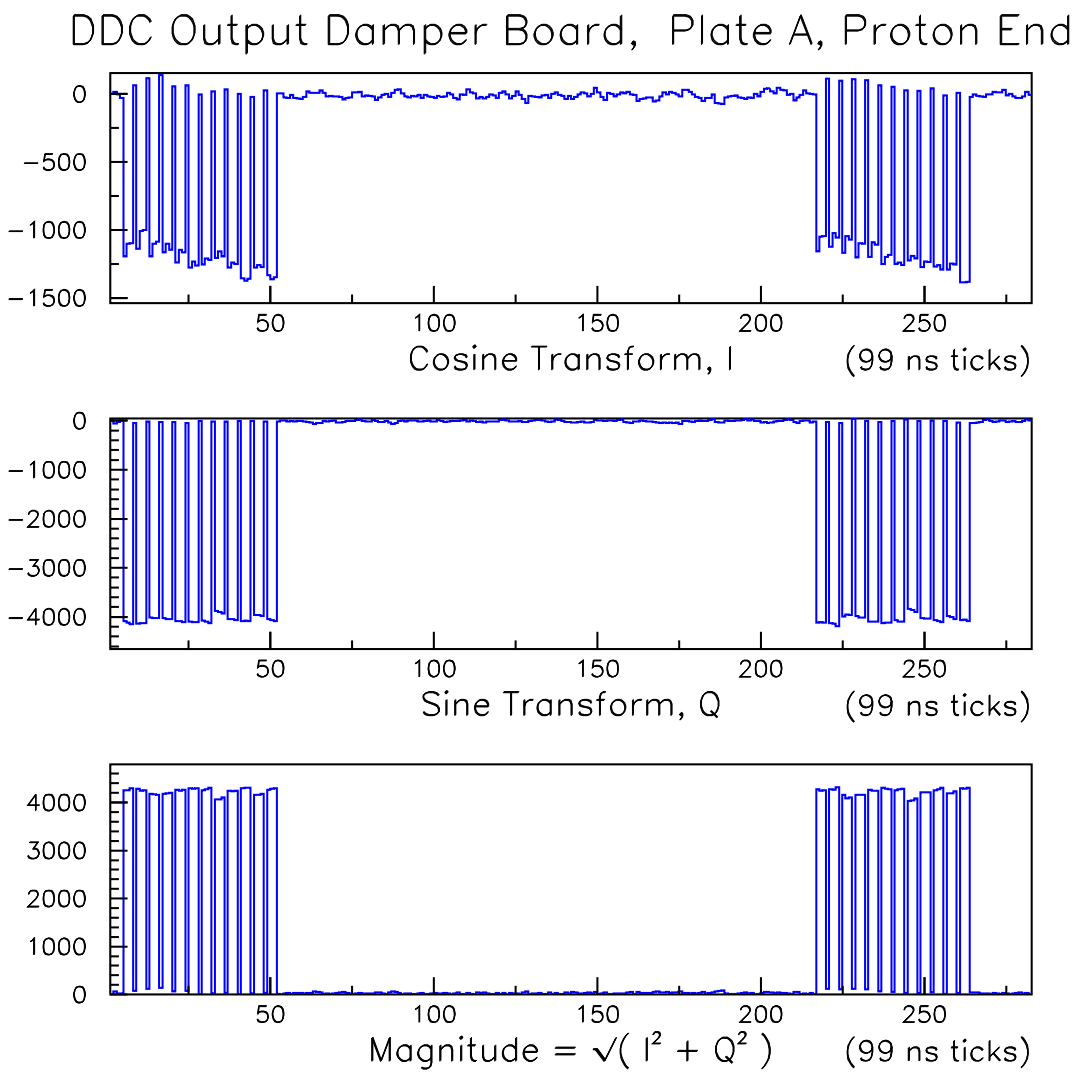

Figure 13: The output of the DDC for about 1.3 turns of the raw data on the p cable. The top plot is the output of the DDC cosine transform, also known as I, and the middle plot is the output of the DDC sine transform, also known as Q. The bottom plot is computed offline and is given by $\sqrt{I^2 + Q^2}$. This DDC algorithm separately resolves each bunch. The 12×0 fill pattern is clear.

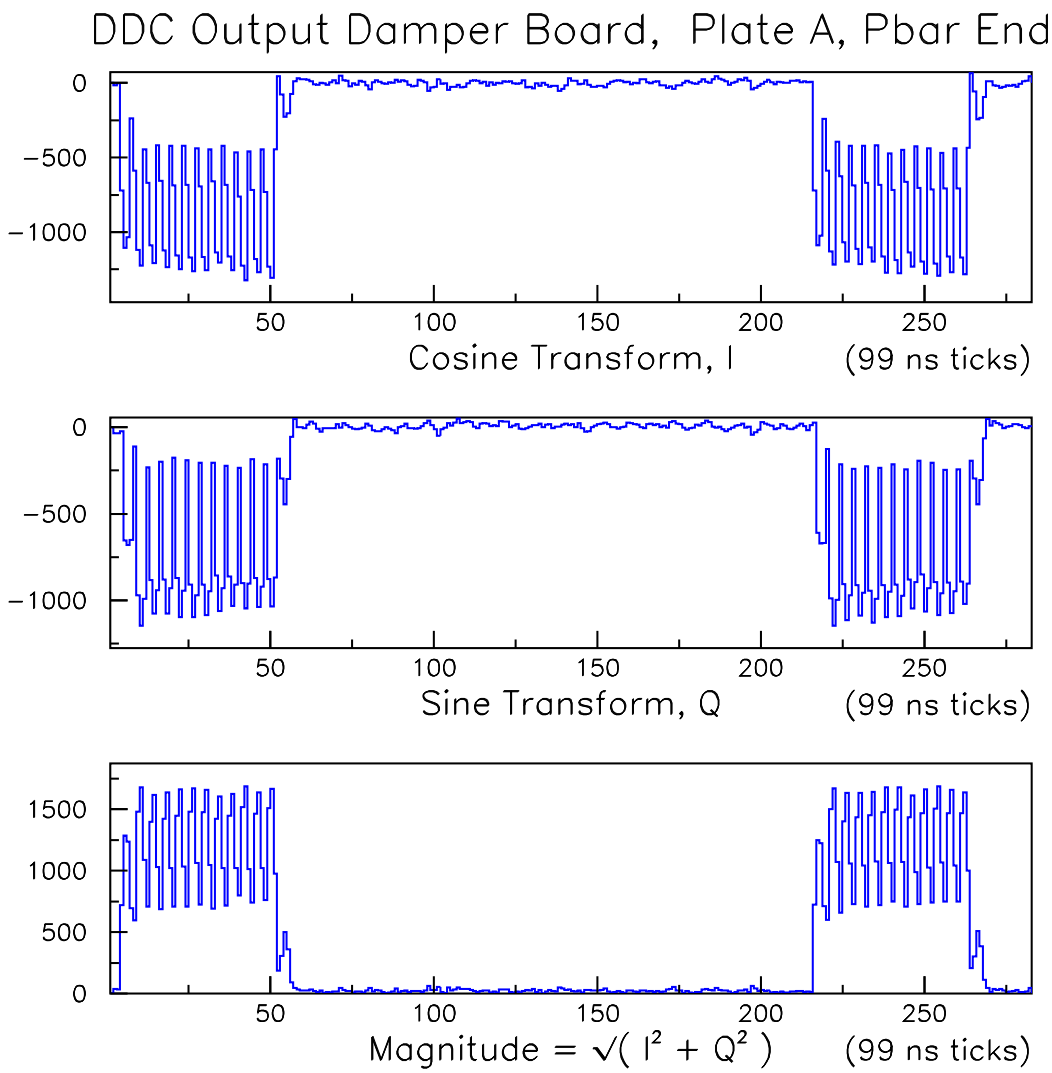

Figure 14: The output of the DDC for about 1.3 turns of the raw data on the $\bar{p}$ cable. The top plot is the output of the DDC cosine transform, also known as I, and the middle plot is the output of the DDC sine transform, also known as Q. The bottom plot is computed offline and is given by $\sqrt{I^2 + Q^2}$. The 12×0 fill pattern is clear. This structure is more complex than the structure on the proton cable, because there are two sources of signal on this cable.

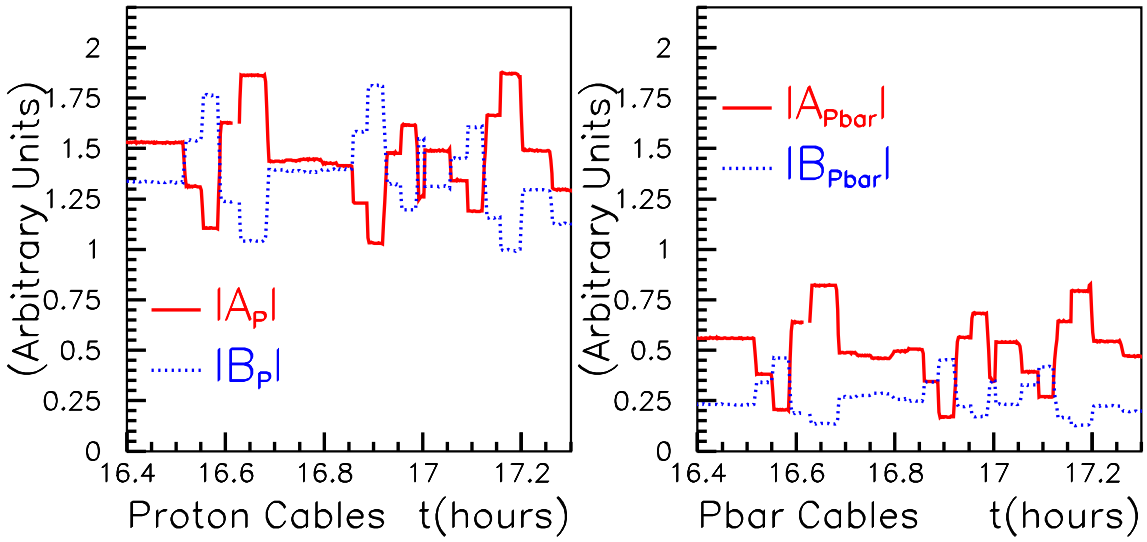

Figure 15: The output of the damper board files for the study described in section 3 and figure 3.

B Processing the Damper Board Data

Each damper board file is processed to extract 4 complex numbers, one for each channel, which will be denoted by $\mathbf{A_p}$, $\mathbf{A_{\bar{p}}}$, $\mathbf{B_p}$, and $\mathbf{B_{\bar{p}}}$, where

$$\Re(\mathbf{A_p}) = \sum_{i=0}^{2047} I_i(A_p) \tag{17}$$

$$\Im(\mathbf{A_p}) = \sum_{i=0}^{2047} Q_i(A_p), \tag{18}$$

and similarly for the other three signals. Ignoring edge effects and an overall phase, $\mathbf{A_p}$ is just three times the Fourier component of the signal on the proton A plate, evaluated at the RF frequency using 9.7 turns of data.

Figure 15 shows the magnitudes of the $\mathbf{A_p}$, $\mathbf{A_{\bar{p}}}$, $\mathbf{B_p}$, and $\mathbf{B_{\bar{p}}}$ signals over a period of about one hour during the study described in section 3 and figure 3.

C Damper Board Data With Both p and $\bar{p}$

Figures figures 11 through through 14 were made for a 12×0 proton only store and were discussed in appendix A. This appendix will present similar plots for a 36×36 store in the afternoon of Dec. 4, 2003. The data were taken using HA15 with the electronics configured as in figure 1.

Figure 16 shows the 12 bunches of one train of protons, as seen on the proton cable from the A plate. Due to a change in the electronics, this data is inverted with respect to the data in figures 11 and 12. It is believed that the inversion comes from the choice of inputs on the damper board, inverting vs non-inverting inputs.

Figure 17 shows the raw data on the $\bar{p}$ cable from the A plate for the same time window as the previous figure. As before, the cables are not phase matched so the time windows may offset from each other by about 35 ns. There are three sets of 12 contributions to this figure: the signals from the 12 bunches of antiprotons; the prompt, non-directional signals from the 12 bunches of protons; and the 12 reflected signals due to the improper termination of the p cable. The first three structures, near 1360, 1444 and 1528 ticks, are signals from three $\bar{p}$ bunches. The fifth structure, near 1612 ticks is the fourth $\bar{p}$ bunch. The structure about half way between the third and fourth $\bar{p}$ bunches, is the prompt, non-directional signal from the first proton bunch. The last structure, underlined in yellow and stretching from about 2580 to 2630 ticks, is the reflection from the last proton bunch, due to improper termination of the proton cable.

The various colored lines were drawn to help interpret the remaining structures. Each set identifies signals from one of the three signal sources and the lines within each set are separated by the bunch spacing. The red vertical lines at the bottom of the plot were drawn starting at the peak bin of the first $\bar{p}$ pulse. The green vertical lines were drawn starting at the peak bin of the prompt, non-directional pulse from the first proton bunch. A horizontal yellow line was drawn underneath the structure near 2600 ticks which is due to the reflections from the proton cable. The other yellow horizontal lines were drawn at the bunch spacing relative to this line.

Clearly the remaining structures in the plot are due to two or three of the signals arriving in time. Recall that the antiprotons are injected in groups of 4 bunches and that the intensity of the bunches decreases with time. The first group of 4 bunches is clearly resolved. The second group of 4 $\bar{p}$ bunches can be resolved above the noise from the protons. But they are much harder to see by eye. From this figure alone it is hard to tell whether or not the final 4 bunches of antiprotons are in the machine. However this can be seen in the bottom left plot of figure 10. In that plot one can see 9 steps in the $\bar{p}$ intensity, corresponding to the $\bar{p}$ injection pattern. So all 36 bunches are present.

These data illustrate a critical scale needed for the design of the BPM system. The signal on the $\bar{p}$ cable which is due to the proton beam is of the same size, or slightly larger, than the signal which comes from the $\bar{p}$ themselves. So, if we want a clean $\bar{p}$ signal with no more than, say 1% contamination, then we need to cancel the proton contribution to less than 1% of itself. This consideration

will be less severe as the antiproton current increases but it the problem of $\bar{p}$ contamination on the p signal will then arise.

For completeness, figures 18 and 19 show the output of the DDC for 1.3 turns of these data.

D Translating the Residual to an Error on Position

Need to write this section.

E Change Log

v1 Original.

v2 Fix error in Figure 1. 3db attentuator on B side was on Pbar and is now on proton where it belongs.

References

[1] "BPM Technology Choice Review", http://wwwserver2.fnal.gov/tevbpm/reviews/tech_choice/.

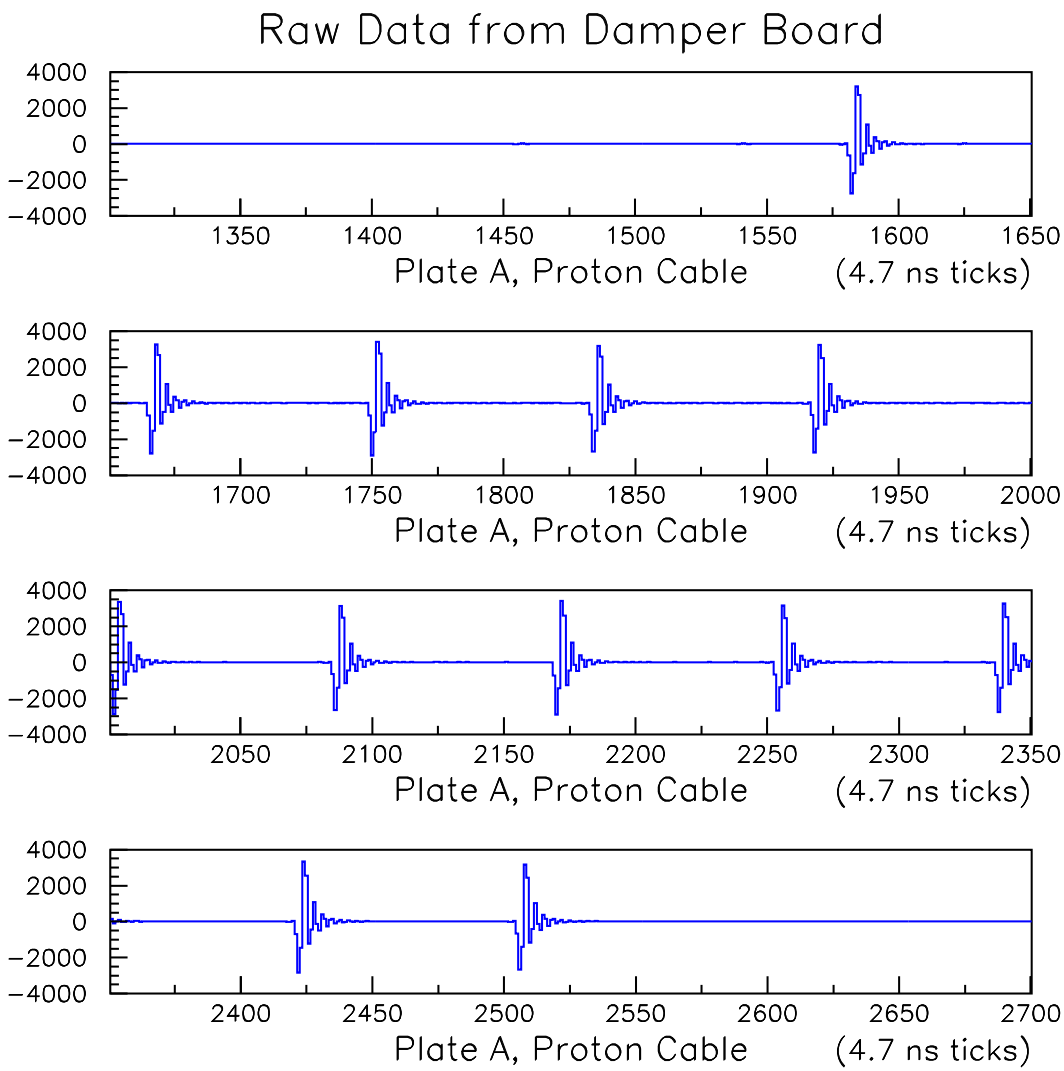

Figure 16: Raw data from the proton cable on plate A for one train of protons. The 4 parts of this figure should be interpreted as one continuous plot. The horizontal axis is time, in units of the digitization clock and the vertical axis is 2× the counts on a ±11 bit ADC (see text for details). The full time scale is about 31% of a turn. The inversion of the signals with respect to those in figure 11 arises from the presence of an extra inverter in one of the configurations.

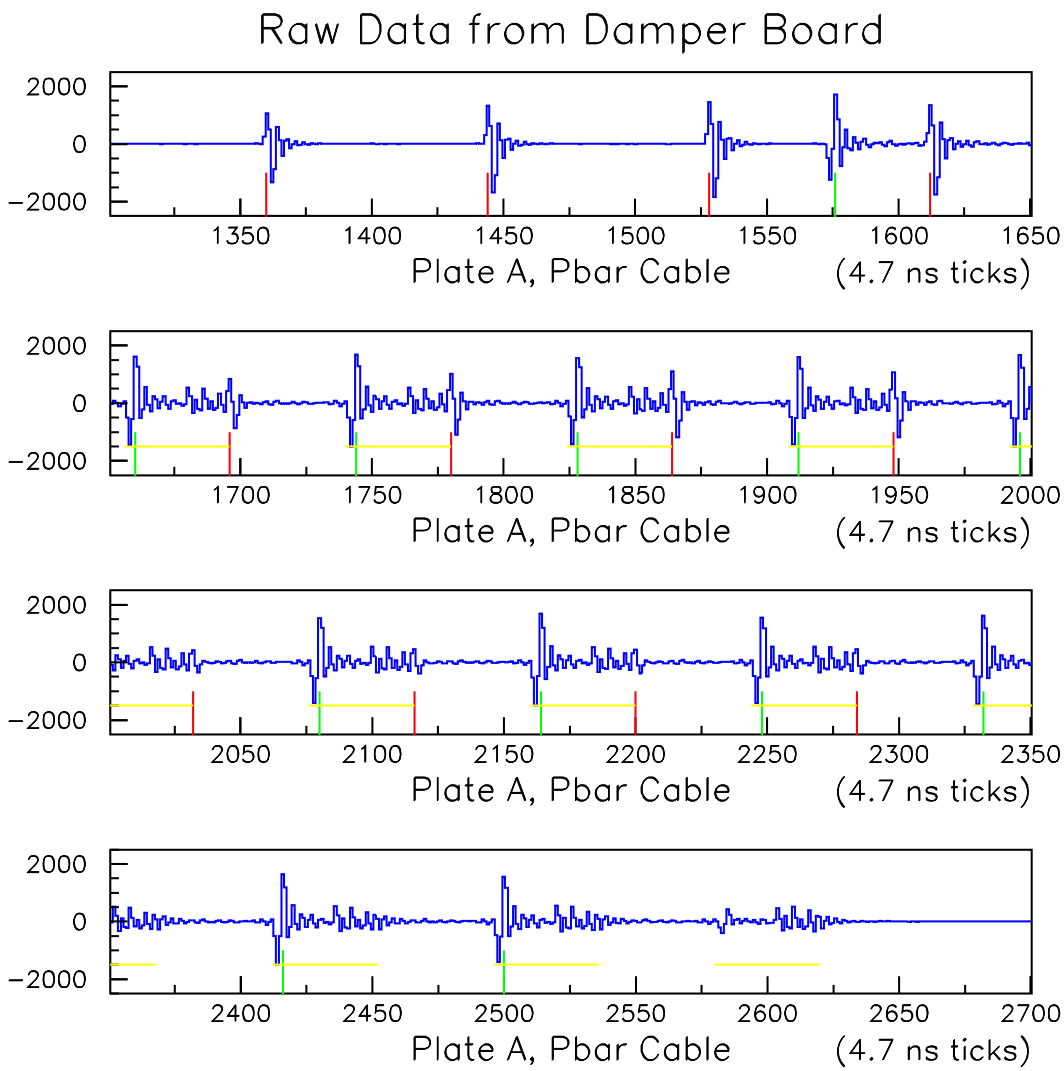

Figure 17: Raw data from the $\bar{p}$ cable on plate A for the same time window as the previous figure. There are three sets of 12 contributions to this figure: the signals from the 12 bunches of antiprotons; the prompt, non-directional signals from the 12 bunches of protons; and the 12 reflected signals due to the improper termination of the p cable. The red, yellow and green lines guide the discussion in the text that identifies which structure comes from which signal source.

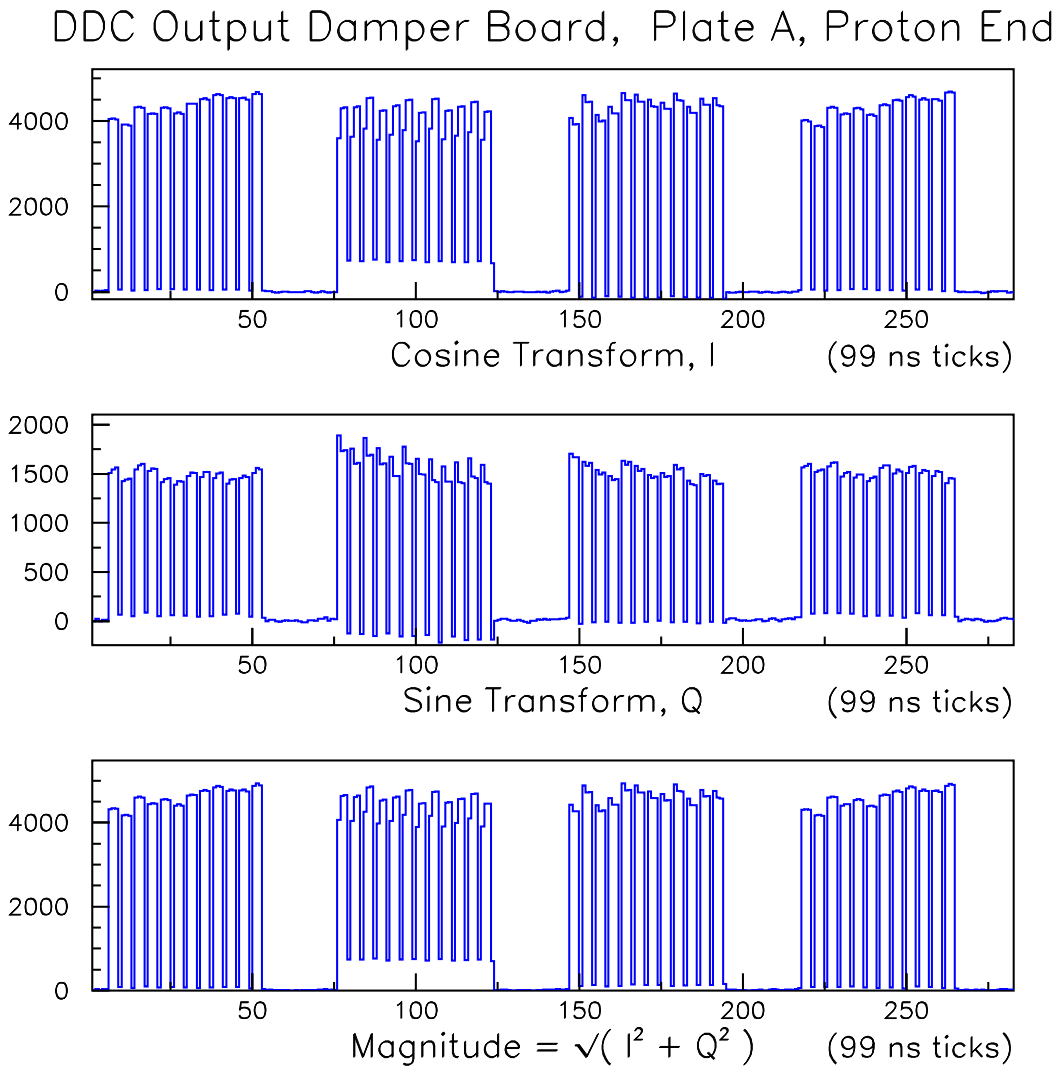

Figure 18: The output of the DDC for about 1.3 turns of the raw data on the p cable for 36×36 running. The top plot is the output of the DDC cosine transform, also known as I, and the middle plot is the output of the DDC sine transform, also known as Q. The bottom plot is computed offline and is given by $\sqrt{I^2 + Q^2}$. The 3 trains of 12 proton bunches are reasonably well resolved. However the individual bunches within second train is not are not as well resolved those within the first and third trains. This is not yet understood.

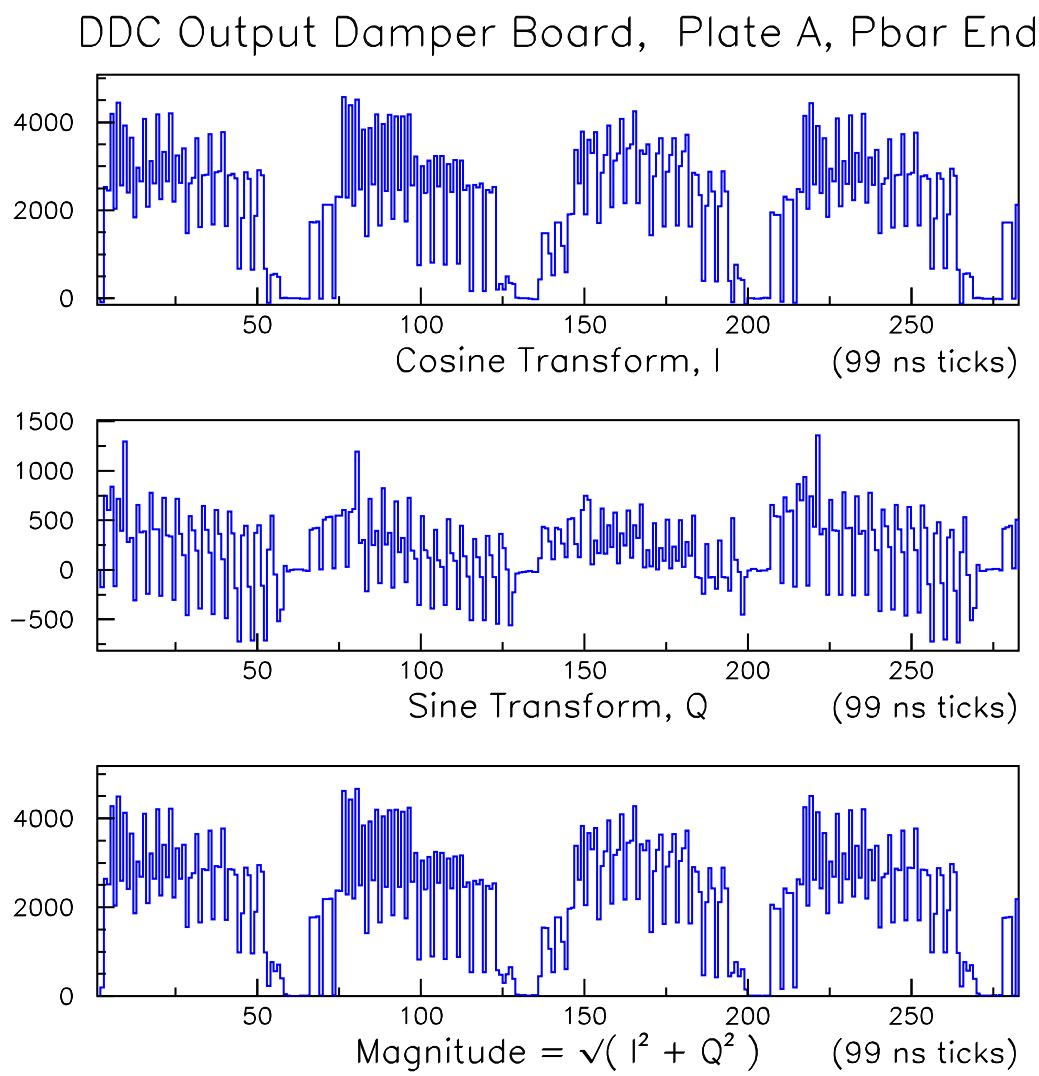

Figure 19: The output of the DDC for about 1.3 turns of the raw data on the $\bar{p}$ cable for 36×36 running. The top plot is the output of the DDC cosine transform, also known as I, and the middle plot is the output of the DDC sine transform, also known as Q. The bottom plot is computed offline and is given by $\sqrt{I^2 + Q^2}$. The trains are reasonably well resolved but the individual bunches in each train are not resolved.